PNAS RESEARCH ARTICLE | CHEMISTRY OPEN ACCESS

A tandem activity-based sensing and labeling strategy reveals antioxidant response element regulation of labile iron pools

Aidan T. Pezacki[a,1], Ryan L. Gonciarz[b,1], Toshitaka Okamura[a], Carson D. Matier[a], Laura Torrente[c], Ke Cheng[b], Sophia G. Miller[d], Martina Ralle[d], Nathan P. Ward[c], Gina M. DeNicola[c], Adam R. Renslo[b,e,2], and Christopher J. Chang[a,f,g,2]

Affiliations are included on p. 9.

Edited by Alison Butler, University of California Santa Barbara, Santa Barbara, CA; received January 23, 2024; accepted May 29, 2024

Iron is an essential element for life owing to its ability to participate in a diverse array of oxidation–reduction reactions. However, misregulation of iron-dependent redox cycling can also produce oxidative stress, contributing to cell growth, proliferation, and death pathways underlying aging, cancer, neurodegeneration, and metabolic diseases. Fluorescent probes that selectively monitor loosely bound Fe(II) ions, termed the labile iron pool, are potentially powerful tools for studies of this metal nutrient; however, the dynamic spatiotemporal nature and potent fluorescence quenching capacity of these bioavailable metal stores pose challenges for their detection. Here, we report a tandem activity-based sensing and labeling strategy that enables imaging of labile iron pools in live cells through enhancement in cellular retention. Iron green-1 fluoromethyl (IG1-FM) reacts selectively with Fe(II) using an endoperoxide trigger to release a quinone methide dye for subsequent attachment to proximal biological nucleophiles, providing a permanent fluorescent stain at sites of elevated labile iron. IG1-FM imaging reveals that degradation of the major iron storage protein ferritin through ferritinophagy expands the labile iron pool, while activation of nuclear factor-erythroid 2-related factor 2 (NRF2) antioxidant response elements (AREs) depletes it. We further show that lung cancer cells with heightened NRF2 activation, and thus lower basal labile iron, have reduced viability when treated with an iron chelator. By connecting labile iron pools and NRF2-ARE activity to a druggable metal-dependent vulnerability in cancer, this work provides a starting point for broader investigations into the roles of transition metal and antioxidant signaling pathways in health and disease.

activity-based sensing | fluorescent iron probe | antioxidant regulation | transition metal signaling | cancer metabolism

Significance

Iron sustains fundamental chemical processes across all kingdoms of life. However, the fluorescence quenching properties and dynamic nature of this metal nutrient make it challenging to study in complex biological systems. We present a tandem activity-based sensing/labeling strategy to enable iron detection with a turn-on fluorescence response and enhanced cellular retention through iron-dependent release of a dye that covalently traps at sites of high iron. This platform reveals complementary expansion or depletion of labile iron pools driven by degradation of ferritin or activation of the nuclear factor-erythroid 2-related factor 2 (NRF2) antioxidant response element, respectively. We further found that cancer cells with heightened NRF2 activation, and thus lower labile iron, are susceptible to iron chelation, establishing a potential druggable metal-dependent vulnerability in cancer.

Iron is an essential metal nutrient that sustains life in large part through its ability to cycle between different oxidation states. This feature facilitates a variety of foundational physiological processes, including oxygen transport, cellular respiration, electron transfer, and nucleotide synthesis (1–4). At the same time, misregulation of iron-dependent redox activity can lead to the generation of harmful reactive oxygen species (ROS) through Fenton chemistry (5), which can induce oxidative stress and ultimately promote a unique cell death pathway, termed ferroptosis, via aberrant peroxidation of polyunsaturated fatty acids (6–9). Indeed, oxidative stress induced by prolonged misregulation of iron has been linked to cancer (10–15), cardiovascular disorders (16), neurodegenerative disorders (17–19), and aging (20). The importance of iron in biology and medicine motivates the development of chemical tools that can effectively monitor this nutrient under different physiological and pathological states. In this context, iron homeostasis is maintained via dynamic stores of intracellular iron, defined as the labile iron pool, where Fe(II) is loosely chelated to cellular ligands for intercellular and intracellular transport. Consequently, this Fe(II) pool represents a proxy for monitoring bioavailable iron status.

Despite the widespread impact of labile iron pools to health and disease, creating methods for Fe(II) detection with requisite metal and oxidation state-specificity, spatial and temporal resolution, and signal-to-noise responses remains a major challenge. Indeed, sensors that employ the traditional binding-based approach (17, 21–26) have shown limited success for Fe(II) as it exhibits low affinity on the Irving-Williams series (27) and is a paramagnetic ion prone to fluorescence quenching through electron and/or energy transfer processes (28, 29). As such, recent efforts have turned to ABS approaches, which exploit the unique reactivity of Fe(II) to enable the selective uncaging of optical reporters in order to elicit a turn-on or ratiometric response (30, 31). Along these lines, we previously designed a Fe(II)-selective trigger based on a 1,2,4-trioxolane (TRX) scaffold inspired by

The authors declare no competing interest.

This article is a PNAS Direct Submission.

[1]A.T.P. and R.L.G. contributed equally to this work.

[2]To whom correspondence may be addressed. Email: adam.renslo@ucsf.edu or chrischang@berkeley.edu.

This article contains supporting information online at https://www.pnas.org/lookup/suppl/doi:10.1073/pnas.2401579121/-/DCSupplemental.

Published July 5, 2024.

clinical-stage antimalarial agents (32). From this starting point, trioxolane-based sensors have been developed for iron imaging using histochemical (33), ratiometric fluorescence (34), bioluminescence (35–38), and positron emission tomography (36, 39) modalities. These reagents complement other ABS strategies for Fe(II) detection reported by our laboratories and others, including N—O oxide reduction (40–46), nitroxide reduction (47), and biomimetic C—O oxidative bond cleavage (48).

Against this backdrop, one major limitation of conventional small-molecule fluorescent probes for iron sensing is that after the activity-based reaction, the reagent can diffuse away from the site of analyte detection. This situation can result in a loss of spatial information concerning local changes in metal fluxes, particularly with regard to reduced signal retention as the reaction product can also diffuse out of the cell. To address this challenge, we now report a tandem activity-based sensing (ABS) and labeling strategy for selective fluorescence imaging of labile iron pools. Iron green-1 fluoromethyl (IG1-FM, Scheme 1 and *SI Appendix*, Scheme S1) reacts selectively with Fe(II) to release a ketone intermediate, which undergoes spontaneous β-elimination to uncage a (N,N′-dimethyl)ethylenediamine linker, followed by self-immolative cyclization to release an *ortho*-fluoromethyl fluorescein dye that rearranges to yield an *ortho*-quinone methide. This highly electrophilic intermediate can covalently anchor to proximal biological nucleophiles to produce a permanent fluorescence mark near the site of analyte detection. IG1-FM is capable of detecting both exogenous and endogenous changes in labile Fe(II) pools in live cells, with a marked increase in signal-to-noise responses over a control IG1 dye or a hydroxymethyl analog that lacks the pendant quinone methide and remains mobile after reaction with Fe(II). We use this sensor to identify and validate that degradation of the major iron storage protein ferritin, known as ferritinophagy, is an essential regulator of intracellular labile Fe(II) status, where disruption of ferritinophagy leads to a decrease in labile Fe(II) pools. We further demonstrate that the sensor is capable of detecting changes in iron bioavailability that are dependent on the degree of activation of the nuclear factor-erythroid 2-related factor 2 (NRF2) transcription factor, where increased activation drives depletion of labile Fe(II) pools in cellular models of lung adenocarcinoma. Additionally, we identify that the dependence of labile iron status on NRF2-antioxidant response element (ARE) activity correlates with susceptibility to cell death induced by iron chelation, as increased NRF2 activation leads to increased sensitivity to iron chelator treatment. By providing a turn-on Fe(II) probe for labile iron pool detection and connecting these stores and NRF2-ARE activity to a druggable metal-dependent vulnerability in cancer, this work provides a starting point for broader investigations into metal and redox cross talk in healthy and disease states.

Results and Discussion

Design and Synthesis of IG1-FM. To develop an ABS iron probe that can preserve intracellular information on bioavailable Fe(II) pools by proximal protein labeling, we coupled the well-validated Fe(II)-responsive TRX trigger for ABS of Fe(II) (33–36, 49) to a modified 3-O-methylfluorescein dye reporter containing a pendant fluoromethyl group *ortho* to the phenolic site of TRX conjugation. We reasoned that Fe(II)-mediated release of a highly electrophilic quinone methide species would allow for proximal covalent reaction of the dye with biological nucleophiles (Scheme 1). While previous reports for hydrogen peroxide or enzyme activity detection appended a reactive trigger directly onto the fluorophore phenol (50–53), direct conjugation of a TRX moiety onto this site would yield an unstable carbonate prone to hydrolysis within biological settings. To overcome this issue, we employed a (N,N'-dimethyl)ethylenediamine linker separating the TRX trigger and dye (15, 37), used previously to cage and release phenolic reporters (37, 54, 55). Upon reaction with Fe(II), the TRX endoperoxide is reduced to a cyclohexanone intermediate, which undergoes spontaneous β-elimination (33) to release an extended amine linker that then undergoes a self-immolative cyclization to uncage the free phenol of the fluorescein payload. Subsequent fluoride elimination generates a highly reactive *ortho*-quinone methide electrophile that is susceptible to attack by proximal biological nucleophiles, resulting in a covalently anchored fluorescent product near the site of activity-based Fe(II) detection (Scheme 1 and *SI Appendix*, Scheme S1). We hypothesized that such a tandem sensing and labeling strategy would enable turn-on Fe(II) detection as the dye is released upon reaction with Fe(II) and thus iron-dependent quenching is minimized. The dye product is also rendered membrane-impermeable, and thus the intracellular fluorescence signal is retained through covalent anchoring to the cell.

We developed a robust synthesis of IG1-FM in six sequential steps from the known (15, 37) enantiopure TRX intermediate **1**, storing and handling the material as the HCl salt to prevent premature self-immolation of the extended linker moiety (Scheme 2). We found that activation of the terminal amine **1** for coupling was best achieved via inverse addition of triethylamine to a reaction mixture containing a large excess of phosgene (~33 equiv.), thereby favoring rapid carbamoylation of the neutralized amine to form **2** and minimizing the competing self-immolation reaction. These optimized conditions enabled shorter reaction times and afforded the carbamoyl halide **2** in high yields of up to 98%. We then coupled intermediate **2** with phenolic 3-formyl fluorescein **S1**, forming a stable dicarbamate linkage between the TRX sensor and the fluorescein dye. Careful reduction of the aldehyde using sodium borohydride at low temperatures ranging from –78 °C to 0 °C afforded alcohol **4,** while preserving the endoperoxide bond of the TRX ring. Finally, conversion of the benzylic alcohol function to fluoromethyl using Deoxo-Fluor proceeded smoothly to afford IG1-FM. Synthesis of IG1, a control probe lacking the fluoromethyl group, was accomplished in four sequential steps. Hence, the phenolic function of fluorescein (**5**) was converted to the *p*-nitrophenylcarbonate intermediate **6**, which was then reacted in situ with *N*-Boc N,N′-dimethylethylenediamine to afford **7** in 45% yield over two steps. Boc deprotection of **7**, followed by

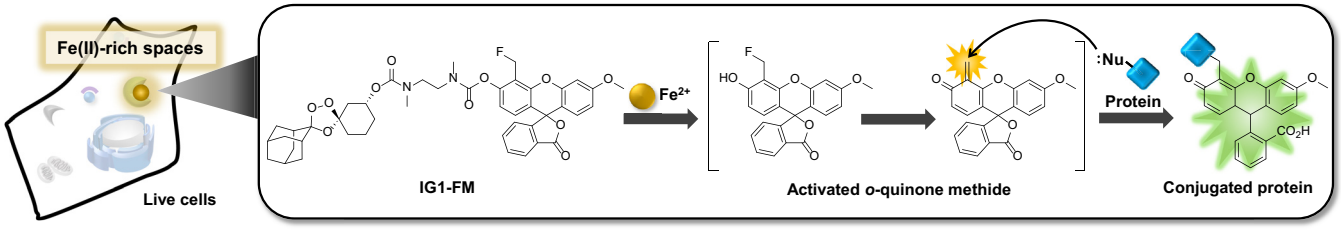

Scheme 1. Design and chemical structure of IG1-FM, a dual tandem ABS and labeling probe for fluorescence detection of labile Fe(II).

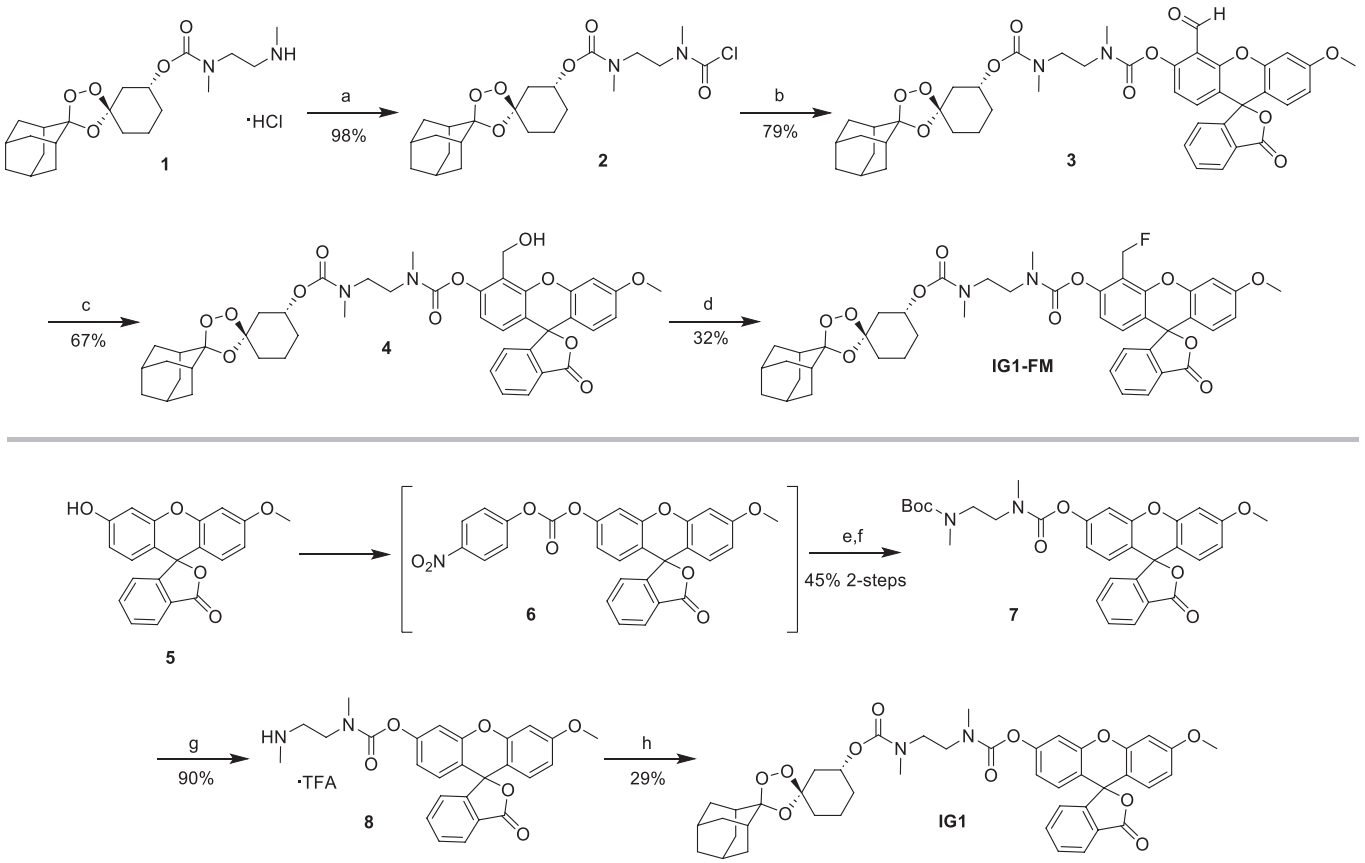

Scheme 2. Synthesis of IG1-FM and control probe IG1. Reagents and conditions: (a) $COCl_2$ (15 wt.% in toluene), NEt_3, CH_2Cl_2, 0 °C to rt, 1.5 h; (b) Compound S1, DMAP, Et_3N, CH_2Cl_2, rt, 4.5 h; (c) $NaBH_4$, THF/EtOH (1:1), −78 °C to 0 °C, 3.5 h; (d) Deoxo-Fluor, 0 °C to rt, 17 h. (e) 4-NO_2PhOC(O)Cl, Et_3N, THF, 0 °C to rt, 1 h; (f) tert-butyl methyl[2-(methylamino)ethyl]carbamate, 0 °C, 15 min; (g) TFA/CH_2Cl_2 (1:1), 0 °C, 40 min; (h) Compound S2 Et_3N, DMF, 0 °C, 2 h 40 min.

coupling of amine **8** with the enantiopure (*R, R*) TRX intermediate **S2** (56) afforded IG1. Lacking the latent *ortho*-quinone methide functionality, this probe served as an important control for evaluating the predicted trapping abilities of IG1-FM.

Fe(II)-Dependent Reactivity and Metal Ion Selectivity of IG1-FM across Aqueous Buffer, Protein, and Proteome Samples. We began by determining the photophysical properties of IG1 and IG1-FM, and their representative reaction products 3-O-Methylfluorescein and Fl-CH_2OH (*SI Appendix*, Table S1). As expected, both IG1 and IG1-FM have relatively low brightness versus their reaction products, suggesting that both sensors are capable of a robust fluorescence turn-on response in a buffered solution upon cleavage of the TRX group. To validate the reactivity of IG1-FM toward Fe(II), we evaluated its fluorescence turn-on responses in aqueous solution buffered to physiological pH with 50 mM 4-(2-hydroxyethyl)-1-piperazineethanesulfonic acid (HEPES). Upon incubation with 10 μM Fe(II), the probe underwent a time-dependent increase in fluorescence (Fig. 1*A*), a feature consistent with other probes that employ quinone-methide chemistry (50–53). Further validation of this product, using liquid chromatography analysis, revealed that it was hydrolyzed to free hydroxymethylfluorescein (Fl-CH_2OH, *SI Appendix*, Figs. S1 and S2). Treatment of IG1-FM with various concentrations of Fe(II) showed a dose-dependent turn-on response for added Fe(II) concentrations spanning 1 to 100 μM. Additionally, coincubation with Fe(II) and the iron-selective chelator deferoxamine (DFO) results in a substantial decrease in fluorescence versus treatment with Fe(II) alone (*SI Appendix*, Fig. S3). The control sensor IG1 similarly showed a dose-dependent response to Fe(II) that was quenchable with DFO (*SI Appendix*, Fig. S4). This turn-on response was also selective for Fe(II) over other biologically relevant metals, including ferric Fe(III) ions, the iron-bound protein myoglobin, or the biologically relevant reductant and oxidant glutathione (GSH) and H_2O_2, respectively (Fig. 1*B*). Moreover, this high selectivity was also retained at various incubation times (*SI Appendix*, Fig. S5). A small fluorescence turn-on response was observed with excess Cu(I) but not at lower, more physiologically relevant copper concentrations. To establish its iron-dependent protein labeling capabilities, we incubated IG1-FM with human serum albumin (HSA) as a model protein in the presence or absence of Fe(II); protein labeling was monitored via sodium dodecyl sulfate–polyacrylamide gel electrophoresis (SDS-PAGE). For 1 to 10 μM of IG1-FM, the HSA-associated fluorescence intensity was elevated in the presence of Fe(II), consistent with Fe(II)-dependent protein labeling by IG1-FM (Fig. 1*C* and *SI Appendix*, Figs. S6 and S7). Analogous protein labeling with HEPG2 cell lysates showed elevations in total lane fluorescence only in the presence of Fe(II), demonstrating the high selectivity for IG1-FM for Fe(II) in whole cellular proteomes (*SI Appendix*, Figs. S8 and S9). We also measured cell lysate labeling efficiency in the presence of excess GSH or various nucleophilic amino acids (*SI Appendix*, Figs. S10 and S11), from which only cysteine had a significant effect on protein labeling. Taken together, these data establish that IG1-FM is a selective and sensitive Fe(II)-responsive fluorescent probe that can undergo protein labeling coupled to activity-based iron sensing.

IG1-FM Is Capable of Imaging Elevation and Depletion of Labile Iron Pools with Metal Supplementation and Chelation in Living Cells. Upon establishing the selectivity and reactivity of

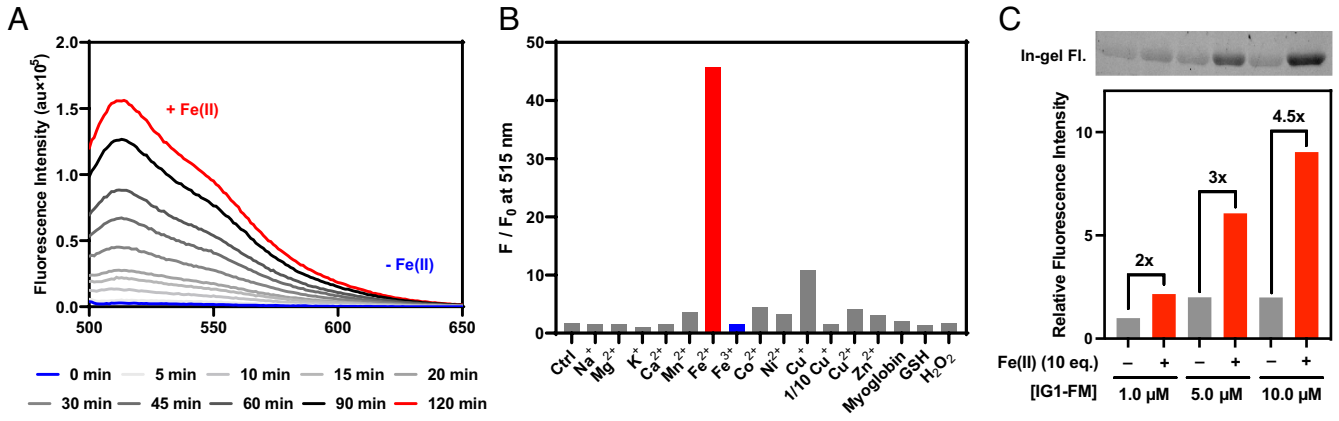

Fig. 1. Reactivity, selectivity, and labeling properties of IG1-FM. (*A*) Time-dependent fluorescence response of 1 μM IG1-FM to 10 μM Fe(II). Spectra were acquired at 37 °C in 50 mM HEPES (pH 7.4) with λ_{ex} = 488 nm, collecting emission between 500 and 650 nm. (*B*) Fluorescence response of 1 μM IG1-FM toward biologically relevant s-block (1 mM) and d-block (10 μM) metals as well as to myoglobin (10 μM), GSH (1 mM), and H_2O_2 (1 mM). Data were acquired at 37 °C in HEPES (pH 7.4) at time = 60 min with λ_{ex} = 488 nm. (*C*) Fe(II)-dependent protein labeling of HAS with IG1-FM. A solution of HSA (0.5 mg/mL) and IG1-FM (1-10 μM) in 50 mM HEPES (pH 7.4) was incubated with or without Fe(II) (10 equiv.) for 30 min and analyzed by SDS-PAGE gel.

IG1-FM for Fe(II) detection, we next sought to evaluate its ability to monitor changes in labile Fe(II) pools in living cells. IG1-FM showed an increased fluorescence response in HEPG2 and U2OS cells preincubated with 100 μM ferrous ammonium sulfate (FAS) as an iron supplement, whereas with the nonfluorinated probes IG1 or the hydroxymethyl compound analog **4**, we saw no fluorescence changes upon treatment with FAS (*SI Appendix*, Figs. S12 and S13). Moreover, we observed that IG1-FM has a more uniform staining pattern compared to IG1, and IG1-FM had a higher basal intracellular fluorescence compared to **4** in HEPG2 cells. Thus, it is likely that IG1-FM provides enhanced cellular retention that is necessary for mapping intracellular labile Fe(II) pools. To further validate this notion, we incubated HEPG2 cells with IG1-FM or the IG1 reaction product 3-O-Methylfluorescein, washed three times with Hank's Balanced Salt Solution (HBSS), and monitored the cellular retention of the probes over the course of 4 h (*SI Appendix*, Figs. S14 and S15). For IG1-FM, we also treated cells with and without FAS to determine whether Fe(II)-dependent differences in signal would persist over time. Indeed, the loss in signal for IG1-FM is minimal over time, only decreasing by approximately 1.3-fold, whereas 3-O-Methylfluorescein has a high initial intracellular fluorescence but dramatically decreases in signal by approximately threefold over 4 h. The poor cellular retention of 3-O-Methylfluorescein may explain the minimal intracellular staining observed with IG1 after reaction with iron. Additionally, we found that the difference in signal for IG1-FM between cells treated with and without exogenous FAS is persistent over the 4-h time course, further demonstrating the utility of the probe in monitoring intracellular labile Fe(II) pools over long time periods. We next monitored changes in labile Fe(II) in HEPG2 cells via external exposure to exogenous iron supplement and/or iron chelator and staining with IG1-FM. To monitor changes in intracellular labile iron induced by external Fe(II) supplementation, we incubated cells with FAS alone or sequentially with the iron chelator DFO followed by FAS. Changes to basal intracellular labile Fe(II) pools were evaluated by incubation of HEPG2 cells with DFO alone or FAS with the hormone hepcidin, which binds and inhibits the iron exporter ferroportin to increase basal intracellular iron levels. As expected, treatment with DFO, or DFO and FAS, produced a significant decrease in IG1-FM fluorescence signal versus basal conditions, while treatment with FAS, or FAS and hepcidin, produced significant increases in IG1-FM fluorescence with the sequential treatment of hepcidin and FAS producing a higher fluorescence signal than treatment with FAS alone (Fig. 2 *A* and *B*). Treatment with hepcidin alone did not result in significant changes in IG1-FM fluorescence (*SI Appendix*, Fig. S16). Analogous chelation treatments were performed with an additional iron chelator bathophenanthroline disulfonate, which produced similar results to those obtained with DFO (*SI Appendix*, Fig. S17). Additionally, we treated HEPG2 cells with various concentrations of FAS and the Fe(III) supplement ferric ammonium citrate (FAC) to test whether higher levels of external iron supplementation would lead to higher levels of intracellular labile iron. While IG1-FM should be unreactive to FAC, a source of Fe(III), the ferric ions may still be imported and reduced to Fe(II) by canonical iron acquisition machinery (57). Thus, treatment with FAC serves as an additional control to rule out the possibility of extracellular activation of IG1-FM. FAS produced fluorescence increases, but total signal reached a maximum at lower metal supplement concentrations (*SI Appendix*, Fig. S18), while treatment with FAC resulted in IG1-FM fluorescence increases that were dose-dependent on the metal supplement concentration (*SI Appendix*, Fig. S19). IG1-FM exhibits minimal cellular toxicity in the presence of iron supplementation/chelation treatments, as confirmed with Hoechst 33342 nuclear stain (*SI Appendix*, Fig. S20). The collective data establish IG1-FM as an effective ABS and labeling probe that is capable of monitoring changes in intracellular labile Fe(II) pools upon metal supplementation and/or chelation.

IG1-FM Identifies Changes in Intracellular Labile Fe(II) Pools Induced by Ferritinophagy. The ability of IG1-FM to monitor both increases and decreases in labile Fe(II) pools upon external addition of metal supplement and/or chelator, along with requisite sensitivity to detect basal levels of intracellular labile Fe(II), led us to interrogate how these metal pools may be affected by other cellular pathways for dynamic iron storage and sequestration. In this context, ferritin is the principal protein responsible for limiting the bioavailability of iron inside cells. A single ferritin can accommodate up to 4,500 iron atoms through the conversion of ferrous ions to ferric oxide via ferroxidase activity and storage in its nano-cage-like protein structure (58). Recent evidence suggests that nuclear receptor coactivator 4 (NCOA4) is responsible for lysosomal uptake and subsequent degradation of ferritin, a process coined as ferritinophagy (59, 60). Additionally, the autophagy receptor Tax1 binding protein 1 (TAX1BP1) has been reported as a NCOA4-binding protein that is required for NCOA4-ferritin trafficking to the lysosome (Fig. 3*A*) (61). Previous studies have

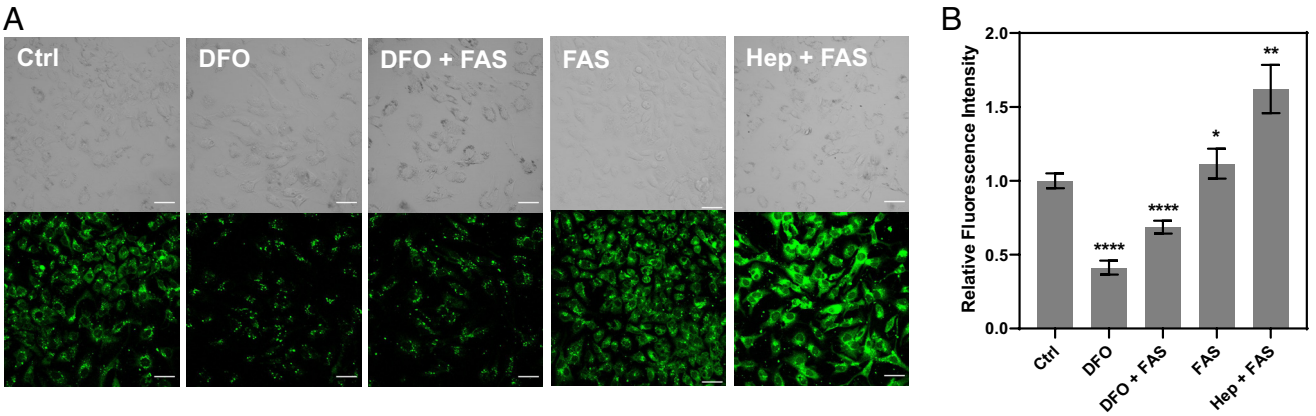

Fig. 2. Fluorescence imaging of labile iron pools in live HEPG2 cells using IG1-FM. (*A*) Confocal microscopy images of HEPG2 cells stained with IG1-FM and treated with vehicle control, DFO for basal Fe chelation, DFO and FAS for chelation of externally supplied Fe, FAS for external Fe supplementation, or FAS and hepcidin for external Fe supplementation and inhibition of iron export. Cells were incubated with vehicle control, 250 μM DFO, or 4 μg/mL hepcidin in low glucose DMEM/10% FBS for 24 h. Medium was then replaced with vehicle control or 100 μM FAS in low glucose DMEM/10% FBS for 90 min, washed once with HBSS (+Ca, Mg) and incubated with 5 μM IG1-FM in HBSS for 1 h. Finally, cells were washed twice with HBSS and then imaged. (*B*) Normalized cellular fluorescence intensities of HEPG2 cells as determined using ImageJ, showing a decrease in signal upon treatment with DFO or DFO with FAS, and an increase in signal in the presence of FAS alone or FAS with Hepcidin. The fluorescence intensity of IG1-FM was determined from experiments performed in triplicate with λ_{ex} = 488 nm. Error bars denote SD (n = 3). (Scale bar, 50 μm.) **P* < 0.1, ***P* < 0.01, and *****P* < 0.0001.

shown that a deficiency in NCOA4 increases basal ferritin levels which in turn limits the bioavailability of intracellular iron (59); however, reports of iron-selective fluorescent imaging applied to directly measure how ferritinophagy regulates labile Fe(II) remain limited (62). Furthermore, whether TAX1BP1 can also regulate intracellular labile Fe(II) levels, and if so, whether it can do so to a comparable degree to NCOA4, remains understudied. Thus, we applied IG1-FM to measure labile Fe(II) pools in HeLa cells with CRISPR-Cas9 generated (63) genetic knockout (KO) of either NCOA4 or TAX1BP1. IG1-FM imaging reveals that both NCOA4 KO and TAX1BP1 KO show lower levels of fluorescence compared to wild-type (WT) cells (Fig. 3 *B* and *C*) suggesting that the disruption of ferritinophagy leads to lower basal levels of labile iron. Interestingly, NCOA4 KO and TAX1BP1 KO show similar reductions in IG1-FM fluorescence when compared with WT cells, indicating that both are essential for the regulation of labile iron via ferritinophagy. We then treated all three cell lines sequentially with FAC to stimulate ferritin production under iron-replete conditions, followed by DFO to stimulate ferritin degradation under iron-deficient conditions, in order to assess whether ferritinophagy could release labile iron from ferritin in response to iron deficiency (Fig. 3*A*). While FAC/DFO treated WT HeLa cells had significantly lower IG1-FM fluorescence compared to controls, the fluorescence for FAC/DFO treated WT cells was still elevated as compared to either of the untreated KO cell lines. These data indicate that ferritinophagy can mitigate iron deficiency by mediating release of sequestered iron stores. Additionally, IG1-FM fluorescence was further reduced in the KO cells upon treatment with FAC and DFO, indicating that the chelator treatment, even in the presence of high ferritin, can promote even further reductions in iron bioavailability.

Interestingly, while we observed complementary decreases in total cellular iron in all three cell lines upon cotreatment with FAC and DFO, as measured by inductively coupled plasma mass spectrometry (ICP-MS), HeLa cells with NCOA4 or TAX1BP1 KO showed reciprocal increases in total iron versus WT HeLa cells (*SI Appendix*, Fig. S21). These findings suggest that a surplus of ferritin results in an overall higher cellular buffering capacity for iron, with a lower level of labile iron. In a key set of control experiments, imaging of HeLa WT cells with the IG1 control probe shows minimal intracellular staining and no significant response upon treatment with FAC and DFO, consistent with data obtained in HEPG2 and U2OS cells (*SI Appendix*, Fig. S22) and highlighting the need for the tandem ABS and labeling in IG1-FM to achieve requisite signal-to-noise responses. Collectively, these data provide direct evidence that NCOA4 and TAX1BP1 modulate intracellular labile Fe(II) pools through ferritinophagy.

IG1-FM Imaging Shows that NRF2 Activation Leads to Depletion of Labile Fe(II) Pools and Higher Susceptibility to Chelation-Induced Cell Death in Cellular Models of Lung Cancer. Having established the utility of IG1-FM to image ferritinophagy-induced changes in intracellular labile Fe(II) levels, we next sought to apply this sensor to biological applications of broader impact and turned our attention to study how cellular antioxidant regulation affects labile iron pool status. In this context, NRF2 is an important transcription factor that up-regulates a variety of detoxifying gene elements, known as AREs, to combat oxidative stress, including several that are associated with iron regulation (64–66). Under basal conditions, NRF2 interacts with its native regulator Kelch-like erythroid cell-derived protein with CNC homology-associated protein 1 (KEAP1), which promotes NRF2 ubiquitination via the Cullin 3-based E3 ligase (Fig. 4*A*) (67). NRF2 is subsequently degraded by the 26S proteasome and maintained at low levels in the cytoplasm (68). In many cancers, NRF2 is aberrantly activated to combat oxidative stress associated with the higher energy demand necessary for the rapid cell division (69–72), while dysregulation of iron homeostasis is also a prominent marker of cancer (73) due to the high demand of iron for cellular processes such as DNA synthesis/repair and energy generation (11, 14, 38). While it has long been speculated that NRF2 activation leads to decreased iron bioavailability as a means to reduce the more damaging effects of oxidative stress, the number of studies that have measured this directly has remained limited (66, 74, 75).

To address this question, we first applied IG1-FM to measure basal intracellular labile Fe(II) levels in lung adenocarcinoma A549 cells with NRF2 KO (NRF2 KO^{+V0}), generated via CRISPR-Cas9 methods (76), versus A549 cells with NRF2 genetic rescue (NRF2 KO^{+NRF2}). A549 cells harbor a loss-of-function mutation in the NRF2 regulator KEAP1 at D236H, and thus genetic rescue of NRF2 should also lead to its activation (77). Interestingly, we observed a marked decrease in labile Fe(II) in NRF2 KO^{+NRF2} cells

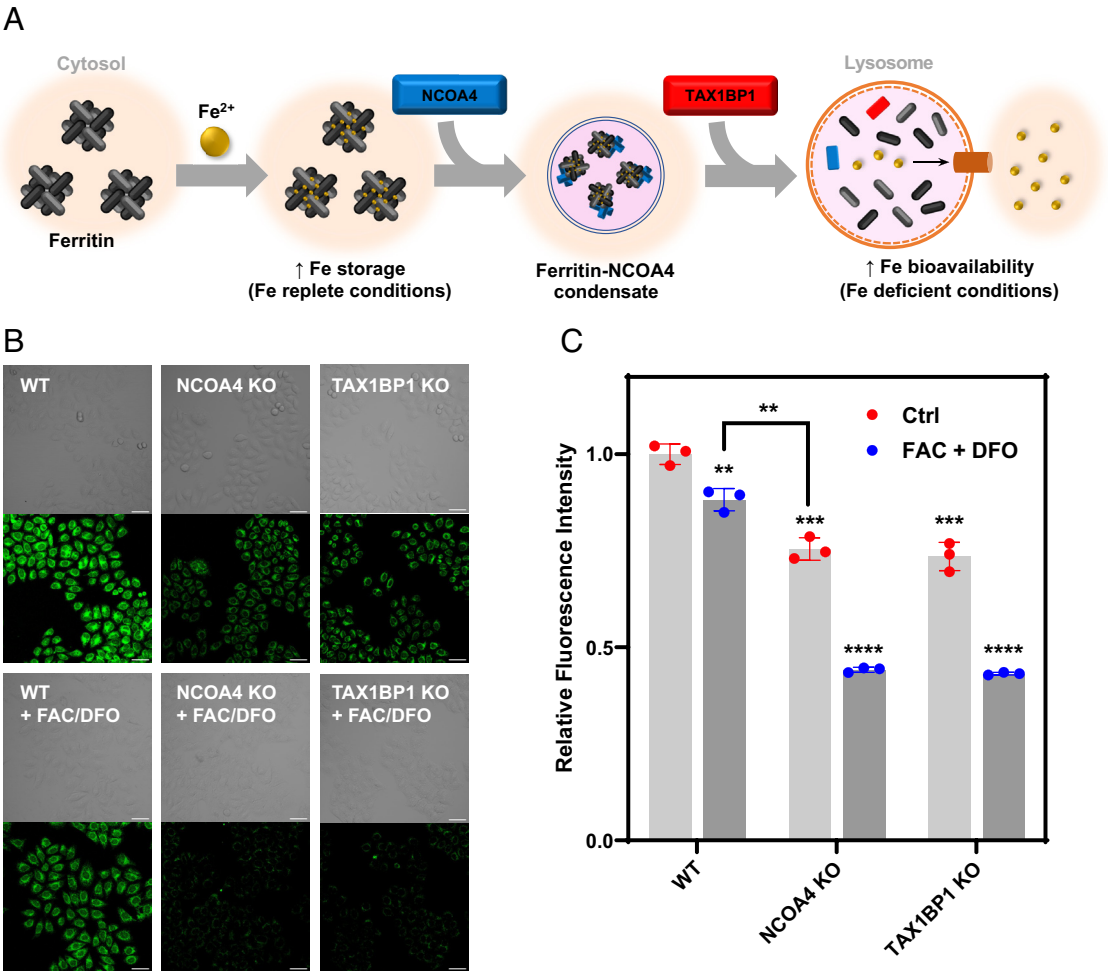

Fig. 3. IG1-FM can detect ferritin-dependent changes in labile Fe(II) pools. (*A*) Model for intracellular iron storage and release, where ferritin sequesters labile Fe(II) and NCOA4/TAX1BP1 mediates ferritinophagy and subsequent iron export back to the cytosol. (*B*) Confocal microscopy images of WT HeLa cells with or without genetic KO of NCOA4 (NCOA4 KO) or TAX1BP1 (TAX1BP1 KO) stained with IG1-FM. Cells were incubated with vehicle control or 50 μM FAC in DMEM/10% FBS for 24 h. Medium was then replaced with vehicle control or 100 μM DFO in DMEM/10% FBS for 24 h, washed once with HBSS (+Ca, Mg), incubated with 5 μM IG1-FM in HBSS for 1 h, and then imaged. (*C*) Normalized cellular fluorescence intensities of HeLa cells as determined using ImageJ, showing a decrease in signal for NCOA4 KO and TAX1BP1 KO and further decreases upon treatment with FAC and DFO. The fluorescence intensity of IG1-FM was determined from experiments performed in triplicate with λ_{ex} = 488 nm. Error bars denote SD (n = 3). (Scale bar, 50 μm.) $^{**}P < 0.01$, $^{***}P < 0.001$, and $^{****}P < 0.0001$.

compared with NRF2 KO^{+V0} control cells (Fig. 4 *B* and *C*), suggesting that NRF2 activation directly regulates intracellular labile iron bioavailability, in agreement with previous findings (66). The decrease in fluorescence signal was supported by complementary ICP–MS measurements of iron to phosphorus ratios, which show a decrease in total cellular iron for A549 cells with NRF2 rescue (*SI Appendix*, Fig. S23). Along these lines, NRF2 would be expected to promote iron export and storage, as ferroportin and ferritin are both ARE-containing genes (65). To better understand how each of these elements may regulate the labile iron pool, we performed RNA sequencing (RNA-seq) on the two NRF2 KO A549 cell lines. Comparing the changes in the NRF2-dependent expression profile, we see elevated gene expression of the two subunits of ferritin (FTH1, ferritin heavy chain 1; FTL, ferritin light chain) and of ferroportin (SLC40A1) in A549 cells with NRF2 KO^{+NRF2} (Fig. 4*D*). The largest changes in expression occur for ferroportin which may explain the overall lower levels of total iron in NRF2 rescue cells, as measured by ICP-MS. Notably, the expression of transferrin receptor (TFRC), which promotes the import of the Fe(III)-bound transferrin complex into cells through receptor-mediated endocytosis (1) but is not an ARE-containing gene, did not change significantly upon genetic rescue of NRF2.

Given that IG1-FM is capable of detecting differences in intracellular labile Fe(II) in cells with complete NRF2 depletion versus NRF2 activation, we next sought to determine whether IG1-FM could be used to profile the relative extent of NRF2 regulation of labile Fe(II) pools across multiple cell lines. While NRF2 activation can result from a surplus of ROS, it can also occur due to mutations in NRF2 or its regulator KEAP1 that impair NRF2-KEAP1 binding and subsequent NRF2 degradation (Fig. 4*A*). These mutations that disrupt the NRF2-KEAP1 interaction are especially frequent in non–small cell lung cancers (NSCLC) and are associated with poor patient prognosis (69, 78, 79). As such, we applied IG1-FM to measure relative intracellular labile Fe(II) levels across a panel of NSCLC cell types with varying degrees of NRF2-KEAP1 interaction. In particular, H1975 and H1299 cells harbor no mutations in KEAP1. In contrast, PC-9 have NRF2 amplification (80), while H460 and H1944 cells harbor G333C and R272L KEAP1 loss-of-function mutations, respectively, that should also promote NRF2 activation. Interestingly, IG1-FM imaging showed a significantly elevated fluorescence signal in H1975 and H1299 cells versus PC-9, H460, and H1944 cells, indicating an overall higher basal level of labile Fe(II) in these cell lines (Fig. 5 *A* and *B* and *SI Appendix*, Fig. S24). Additionally,

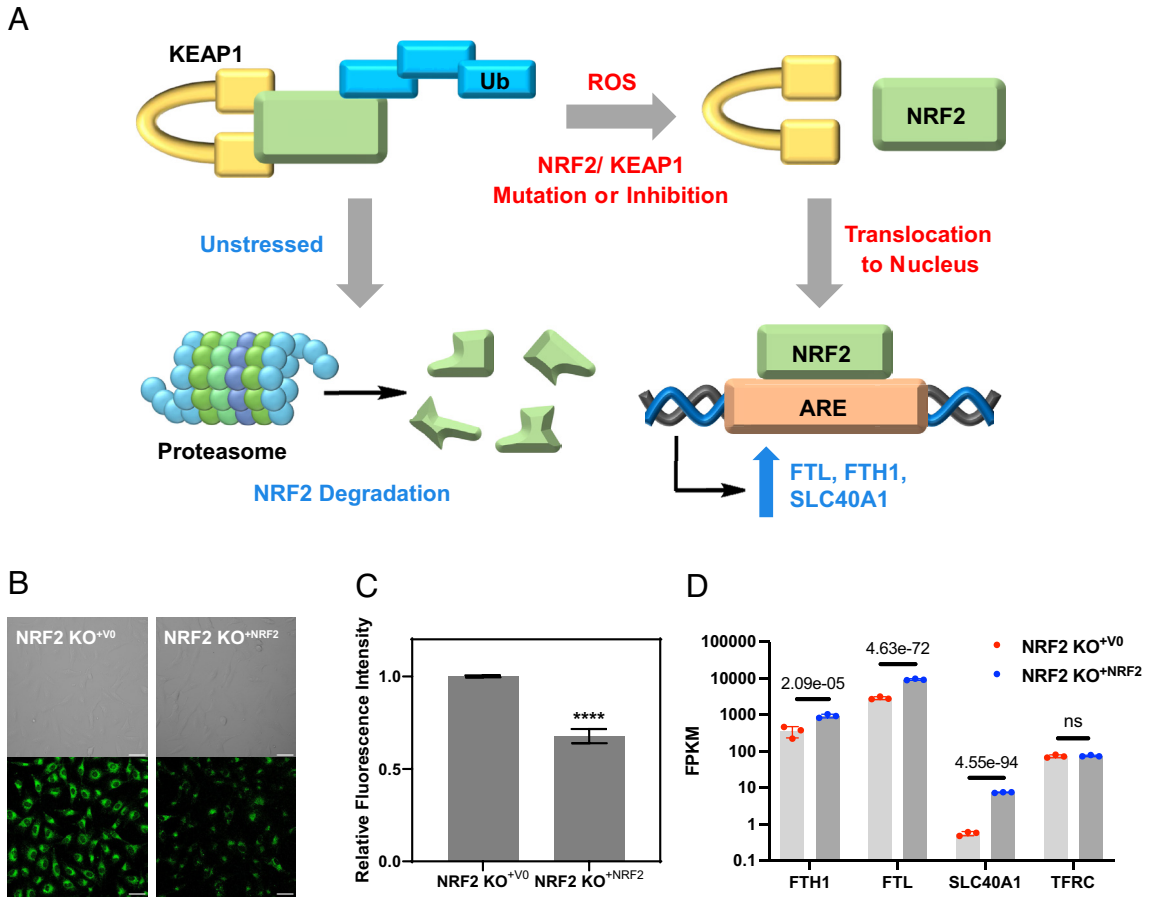

Fig. 4. Live-cell imaging with IG1-FM identifies a reciprocal relationship between labile iron pools and activation of AREs, where decreased levels of labile Fe(II) pools are observed upon greater activation of the ARE transcription factor regulator, NRF2. (*A*) Model for intracellular regulation and activation of NRF2, where elevated ROS, mutations in NRF2/KEAP1, or inhibition of the NRF2-KEAP1 interaction promotes NRF2 activation, which in turn sequesters labile Fe(II) via increased expression of iron regulatory proteins. (*B*) Confocal fluorescence microscopy images of A549 cells stably expressing NRF2 KO^{+V0} or NRF2 KO^{+NRF2}. Cells were washed once with HBSS, incubated with IG1-FM for 1 h, and then imaged. (*C*) Normalized mean IG1-FM fluorescence intensity of A549 cells showing a decrease in signal for NRF2 KO^{+NRF2} versus NRF2 KO^{+V0}. Error bars denote SD (n = 3). The fluorescence intensity of IG1-FM was determined from experiments performed in triplicate with λ_{ex} = 488 nm. (Scale bar, 50 μm.) ***$P < 0.001$. (*D*) Expression levels of labile iron regulating AREs and TFRC in A549 cells stably expressing NRF2 KO^{+V0} or NRF2 KO^{+NRF2}. Expression levels are presented as fragments per kilobase of transcript per million mapped reads (FPKM) and were determined from experiments performed in triplicate. Statistical significance is presented as adjusted *P*-values. ns, not statistically significant.

treatment with the KEAP1 inhibitor KI-696 resulted in decreases in IG1-FM signal only in H1975, H1299, and PC-9 cells, all of which have WT KEAP1, while KI-696 produced no significant difference in H460 and H1944 cells with KEAP1 mutations. To confirm these measurements, we performed analogous imaging with RhoNox-4, an ABS probe which utilizes different reaction chemistry for detection of labile Fe(II) (81), and TRX-Puro, a histochemical TRX probe whose signal can be normalized via treatments with free puromycin (33). Both RhoNox-4 and TRX-Puro showed similar trends in labile Fe(II) across the NSCLC panel with higher signals for H1975 and H1299 cells, and signal decreases upon treatment with KI-696 only for H1975, H1299, and PC-9 cells (*SI Appendix*, Figs. S25 and S26). These results suggest that NRF2 activity can directly correlate with the bioavailability of intracellular labile Fe(II). Unlike the NRF2 KO A549 cells lines, all NSCLC cell lines showed no significant changes in total iron upon KEAP1 inhibition via KI-696 aside from H1299 cells, which exhibited a slight increase (*SI Appendix*, Fig. S27). Additionally, whereas cell lines with NRF2 amplification or KEAP1 mutations had higher levels of total iron compared to KEAP1 WT cells, these differences were modest. Given this disparity with expression changes seen for A549 cells, we suspected that these cell lines possess different ARE gene expression profiles with greater promotion of proteins involved in iron storage and/or uptake. To confirm this hypothesis, we performed RNA-seq on H1975 cells and compared the expression levels of FTH1, FTL, SLC40A1, and TFRC between the two conditions. Upon treatment with KI-696, the most marked changes in gene expression occurred for FTH1 and FTL (*SI Appendix*, Fig. S28), while TFRC also witnessed a small increase in expression, likely due to stabilization of iron-responsive-element-binding proteins (82). These expression profiles suggest that there is a finely tuned balance between iron export, import, and storage in these cells. This homeostatic balance produces overall smaller changes in total iron concentrations, while still decreasing labile iron pools. Indeed, an elevation in either or both iron storage and export will lower its bioavailability and likely outweigh the increased contributions of labile iron from increased TFRC. These results are also in agreement with those of HeLa cells where inhibition of ferritinophagy via NCOA4 KO or TAX1BP1 KO leads to reduced labile iron but elevated total iron.

Finally, we hypothesized that NSCLC cells that possess lower basal labile iron due to NRF2 amplification or KEAP1 mutations would have heightened sensitivity to iron chelation compared to cells with WT KEAP1. Indeed, NRF2 expression has been previously shown to correlate positively with resistance to ferroptosis in a panel of different ovarian cancer cell lines (66). To test this notion, we treated this panel of NSCLC cells with DFO and

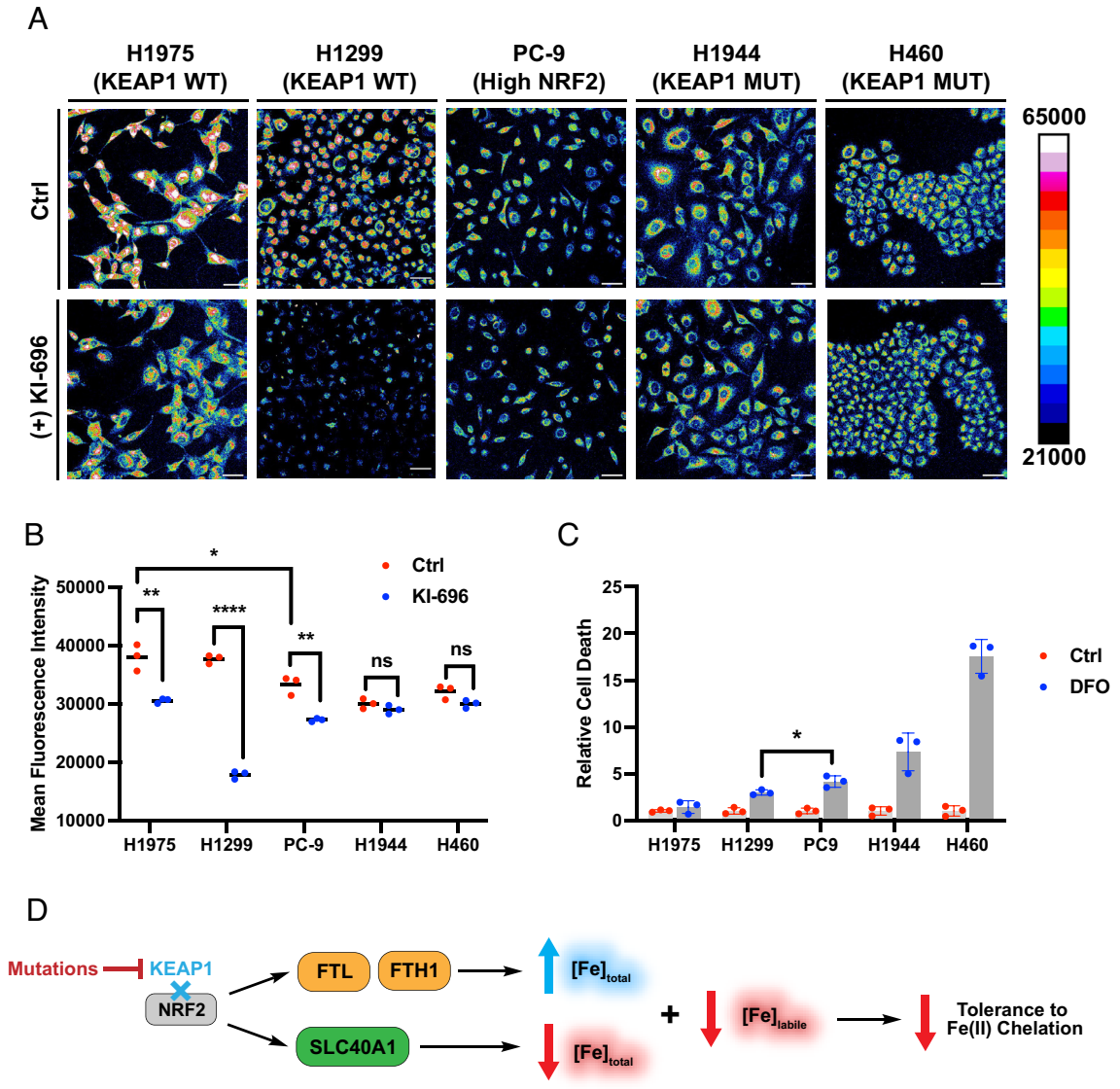

Fig. 5. Mutations or inhibition of KEAP1 lead to reduced levels of intracellular labile Fe(II) pools. (*A*) Confocal fluorescence images of IG1-FM in NSCLC cell lines with KEAP1 WT, WT KEAP1 and high levels of NRF2 (High NRF2), or mutant KEAP1 (KEAP1 MUT), treated with and without a KEAP1 inhibitor (KI-696). Cells were incubated with vehicle control or 1 μM KI-696 in RPMI 1640/10% FBS for 48 h. Cells were then washed once with HBSS, incubated with IG1-FM for 1 h, and imaged. (*B*) Mean IG1-FM fluorescence intensity of NSCLC cells showing a higher signal for KEAP1 WT cells over high NRF2 or KEAP1 MUT cells, and further decreases in signal upon treatment with KI-696 only for cells with KEAP1 WT. Error bars denote SD (n = 3). The fluorescence intensity of IG1-FM was determined from experiments performed in triplicate with λ_{ex} = 488 nm. (Scale bar, 50 μm.) (*C*) Relative cell death of NSCLC cell lines treated with vehicle control or DFO, showing cells with high NRF2 activation or KEAP1 mutations have higher sensitivities to iron chelation compared to cells with KEAP1 WT. Cells were incubated with vehicle control or 100 μM DFO in RPMI 1640/10% FBS over 72 h and cell death was monitored via Sytox Green, as previously described (83). *P < 0.1, **P < 0.01, ***P < 0.001, and ****P < 0.0001; ns, not statistically significant. (*D*) Proposed model of how NRF2 activation drives sensitivity to iron chelation in NSCLC cells. Loss-of-function mutations in KEAP1 induce NRF2 activation, which can then cause heightened expression of FTL/FTH1 and/or SLC40A, in turn leading to aberrant decreases in labile iron that serve as a druggable metal-dependent disease vulnerability.

monitored cell death over 72 h. While H1299 cells showed modest cell death upon chelation treatment, PC-9, H1944, and H460 had significantly elevated cell death compared to both H1975 and H1299 cells (Fig. 5*C* and *SI Appendix*, Fig. S29). Taken together, the data show that IG1-FM can be used as a tool to profile intracellular labile Fe(II) levels and reveal a reciprocal relationship between NRF2-ARE activation and labile Fe(II) pools that can be exploited as a unique metal-dependent vulnerability to selectively target cancer cells with hyperactivated NRF2 via iron chelation treatment (Fig. 5*D*).

Concluding Remarks. We have presented the design, synthesis, and biological evaluation of a first-generation probe for fluorescence imaging of intracellular labile iron pools using a tandem ABS and labeling strategy. We leveraged the combination of a selective and sensitive TRX-based trigger for ABS of Fe(II) in combination with *ortho*-quinone-methide chemistry for protein labeling to generate IG1-FM, a green fluorescent probe for imaging intracellular labile iron pools. By installing a self-immolative linker between the analyte-responsive element and the fluoromethyl dye reporter, we anticipate that this quinone-methide chemistry will be broadly applicable for other ABS strategies featuring scaffolds with limited cellular retention. Such strategies may include further tuning of the chemical reporter to enable development of probes with red-shifted fluorescence emission, different imaging modalities, enrichment handles for -omics studies, and/or therapeutic payloads.

IG1-FM achieves a selective and sensitive Fe(II)-dependent fluorescence turn-on response, enabling the detection of changes in intracellular labile Fe(II) in live cells upon iron supplementation, iron chelation, and/or iron-dependent hormone (hepcidin)

treatments. Experiments with the control reagents IG1 or hydroxymethyl **4** that do not possess the latent quinone methide group show the essential nature of the dual sensing/labeling moiety to trap the probe inside the cell to obtain robust signal-to-noise responses. Moreover, the enhanced cellular retention obtained using IG1-FM advances the study of foundational aspects of iron biology. In one example, we established that intracellular labile Fe(II) pools are directly regulated by ferritinophagy. Genetic depletion of the ferritin-binding protein NCOA4 or the autophagy receptor TAX1BP1 both resulted in decreased IG1-FM fluorescence, suggesting that degradation of ferritin can directly contribute to the native intracellular labile Fe(II) pool. Further investigations may explore how inhibition of ferritinophagy may affect subcellular localization of labile Fe(II) pools, or whether overexpression of ferritinophagy-associated proteins may impact basal iron levels. Additionally, elucidating how NCOA4 may regulate other forms of labile iron, such as that incorporated into labile heme, would be of additional future interest.

We also used IG1-FM to reveal that NRF2-ARE activation regulates the bioavailability of intracellular labile Fe(II) pools in cellular models of cancer, where we identify a reciprocal relationship in which a greater extent of NRF2 activation drives lower levels of intracellular labile Fe(II) pools across various lung cancer cell lines. We speculate that upregulation of ferroportin and ferritin, which can contribute to iron export and sequestration, respectively, in NRF2-ARE pathways play important biochemical roles, but because NRF2 can also regulate TFRC, heme oxygenase-1, both of which can increase labile iron, and can indirectly control ferritin levels through HECT and RLD domain containing E3 ubiquitin protein ligase 2 and vesicle-associated membrane protein 8 (66), this situation is likely to be mechanistically complex. As such, the outstanding question of how all AREs may impact labile Fe(II) independently remains to be fully deciphered. More broadly, our findings presage that cross talk between labile iron and NRF2-ARE signaling may be an important prognostic marker and a therapeutic target in cancer initiation and progression. Notably, we show that cells with NRF2 amplification or KEAP1 loss-of-function mutations have higher rates of cell death when treated with iron chelator than cells with WT KEAP1. This finding identifies a promising therapeutic strategy to target this iron-dependent disease vulnerability, as cancers with heightened NRF2 activity may be selectively treated while minimizing off-target effects against healthy tissue where NRF2 is maintained at low concentrations with minimal activation. Altogether, this work provides a starting point for further investigations into how iron as a transition metal signal (84) may contribute to metal-dependent disease vulnerabilities by spatial, temporal, and redox control.

Materials and Methods

Full materials and procedures for the synthesis of compounds, spectroscopic characterization, cellular imaging, generation of cell lines, and cell analysis are described in *SI Appendix*. Fluorescence spectra and metal ion selectivity were measured using a PTI QuantaMaster 400 fluorimeter (Horiba). Reaction trace monitoring was carried out using an Agilent 1260 Infinity II System with an InfinityLab LC/MSD XT (column: EC-C18, 120 Å, 2.7 μm, 4.6 × 100 mm, method: 0 to 8 min 5 to 100% MeCN with 0.1% FA in H_2O with 0.1% FA, 8 to 12 min hold at 100% MeCN with 0.1% FA, flow rate 1,500 mL/min). Live cells were maintained as a monolayer in exponential growth at 37 °C in a 5% CO_2 atmosphere. For confocal fluorescence imaging, cells were seeded at 30% confluency in 8-well chamber slides (Ibidi), allowed to grow to 70% confluency prior to imaging, and were imaged using a Zeiss LSM880 laser scanning confocal microscopy system with a 20× dry objective lens, and images were analyzed using Fiji (NIH).

Data, Materials, and Software Availability. All study data are included in the article and/or *SI Appendix*.

ACKNOWLEDGMENTS. We thank the NIH (GM79465 and GM139245 to C.J.C.; AI105106 to A.R.R.) the Florida Department of Health (9BC07 to G.M.D.), and the Agilent Biodesign Program (to C.J.C.) for support of this work. C.J.C. is a CIFAR Fellow. We thank Dr. Alison Killilea, Willie S. Hercule, and Sara E. Sosa (University of California, Berkeley Tissue Culture Facility) for expert technical assistance; Dr. Laura Craciun for helpful discussions; and Prof. Noboru Mizushima (The University of Tokyo) and Prof. Hayashi Yamamoto (Nippon Medical School) for sharing NCOA4 and TAX1BP1 KO HeLa cell lines. ICP-MS measurements were performed in the OHSU Elemental Analysis Core with partial support from the NIH (S10OD028492). The 600 MHz cryoprobe (University of California, Berkeley College of Chemistry NMR Facility) was supported by NIH (S10OD024998).

Author affiliations: [a]Department of Chemistry, University of California, Berkeley, CA 94720; [b]Department of Pharmaceutical Chemistry, University of California, San Francisco, CA 94158; [c]Department of Metabolism and Physiology, H. Lee Moffitt Cancer Center and Research Institute, Tampa, FL 33612; [d]Department of Molecular and Medical Genetics, Oregon Health & Science University, Portland, OR 97239; [e]Helen Diller Family Comprehensive Cancer Center, University of California, San Francisco, CA 94158; [f]Department of Molecular and Cell Biology, University of California, Berkeley, CA 94720; and [g]Helen Wills Neuroscience Institute, University of California, Berkeley, CA 94720

Author contributions: A.T.P., R.L.G., T.O., C.D.M., N.P.W., G.M.D., A.R.R., and C.J.C. designed research; A.T.P., R.L.G., T.O., S.G.M., and N.P.W. performed research; A.T.P., R.L.G., T.O., C.D.M., L.T., and K.C. contributed new reagents/analytic tools; A.T.P., R.L.G., S.G.M., M.R., N.P.W., G.M.D., A.R.R., and C.J.C. analyzed data; and A.T.P., R.L.G., A.R.R., and C.J.C. wrote the paper.

1. M. W. Hentze, M. U. Muckenthaler, N. C. Andrews, Balancing acts: Molecular control of mammalian iron metabolism. *Cell* **117**, 285–297 (2004).
2. R. Cammack, J. M. Wrigglesworth, H. Baum, "Iron-dependent enzymes in mammalian systems" in *Transport and Storage*, P. Ponka, H. M. Schulman, R. C. Woodworth, G. W. Richter, Eds. (CRC Press, 1989), p. 17.
3. S. J. Lippard, J. M. Berg, *Principles of Bioinorganic Chemistry* (University Science Books, 1994).
4. D. C. Johnson, D. R. Dean, A. D. Smith, M. K. Johnson, Structure, function, and formation of biological iron-sulfur clusters. *Annu. Rev. Biochem.* **74**, 247–281 (2005).
5. C. C. Winterbourn, Toxicity of iron and hydrogen peroxide: The Fenton reaction. *Toxicol. Lett.* **82-83**, 969–974 (1995).
6. S. J. Dixon *et al.*, Ferroptosis: An iron-dependent form of nonapoptotic cell death. *Cell* **149**, 1060–1072 (2012).
7. X. Jiang, B. R. Stockwell, M. Conrad, Ferroptosis: Mechanisms, biology and role in disease. *Nat. Rev. Mol. Cell Biol.* **22**, 266–282 (2021).
8. S. J. Dixon, D. A. Pratt, Ferroptosis: A flexible constellation of related biochemical mechanisms. *Mol. Cell* **83**, 1030–1042 (2023).
9. Z. Li, M. Lange, S. J. Dixon, J. A. Olzmann, Lipid quality control and ferroptosis: From concept to mechanism. *Annu. Rev. Biochem.*, 10.1146/annurev-biochem-052521-033527 (2024).
10. Z. K. Pinnix *et al.*, Ferroportin and iron regulation in breast cancer progression and prognosis. *Sci. Transl. Med.* **2**, 43ra56 (2010).
11. S. V. Torti, F. M. Torti, Iron and cancer: More ore to be mined. *Nat. Rev. Cancer* **13**, 342–355 (2013).
12. D. H. Manz, N. L. Blanchette, B. T. Paul, F. M. Torti, S. V. Torti, Iron and cancer: Recent insights. *Ann. N. Y. Acad. Sci.* **1368**, 149–161 (2016).
13. D. Basuli *et al.*, Iron addiction: A novel therapeutic target in ovarian cancer. *Oncogene* **36**, 4089–4099 (2017).
14. R. Rodriguez, S. L. Schreiber, M. Conrad, Persister cancer cells: Iron addiction and vulnerability to ferroptosis. *Mol. Cell* **82**, 728–740 (2022).
15. R. L. Gonciarz *et al.*, Elevated labile iron in castration–resistant prostate cancer is targetable with ferrous iron–activatable antiandrogen therapy. *Eur. J. Med. Chem.* **249**, 115110 (2023).
16. S. von Haehling, E. A. Jankowska, D. J. van Veldhuisen, P. Ponikowski, S. D. Anker, Iron deficiency and cardiovascular disease. *Nat. Rev. Cardiol.* **12**, 659–669 (2015).
17. E. L. Que, D. W. Domaille, C. J. Chang, Metals in neurobiology: Probing their chemistry and biology with molecular imaging. *Chem. Rev.* **108**, 1517–1549 (2008).
18. D. Hare, S. Ayton, A. Bush, P. Lei, A delicate balance: Iron metabolism and diseases of the brain. *Front. Aging Neurosci.* **5**, 34 (2013).
19. C. J. Chang, Bioinorganic life and neural activity: Toward a chemistry of consciousness? *Acc. Chem. Res.* **50**, 535–538 (2017).
20. R. J. Ward, F. A. Zucca, J. H. Duyn, R. R. Crichton, L. Zecca, The role of iron in brain ageing and neurodegenerative disorders. *Lancet Neurol.* **13**, 1045–1060 (2014).
21. D. W. Domaille, E. L. Que, C. J. Chang, Synthetic fluorescent sensors for studying the cell biology of metals. *Nat. Chem. Biol.* **4**, 168–175 (2008).
22. K. P. Carter, A. M. Young, A. E. Palmer, Fluorescent sensors for measuring metal ions in living systems. *Chem. Rev.* **114**, 4564–4601 (2014).

23. D. J. Hare, E. J. New, M. D. de Jonge, G. McColl, Imaging metals in biology: Balancing sensitivity, selectivity and spatial resolution. *Chem. Soc. Rev.* **44**, 5941–5958 (2015).
24. A. T. Aron, K. M. Ramos-Torres, J. A. Cotruvo, C. J. Chang, Recognition- and reactivity-based fluorescent probes for studying transition metal signaling in living systems. *Acc. Chem. Res.* **48**, 2434–2442 (2015).
25. C. M. Ackerman, S. Lee, C. J. Chang, Analytical methods for imaging metals in biology: From transition metal metabolism to transition metal signaling. *Analyt. Chem.* **89**, 22–41 (2017).
26. E. J. New, V. C. Wimmer, D. J. Hare, Promises and pitfalls of metal imaging in biology. *Cell Chem. Biol.* **25**, 7–18 (2018).
27. H. Irving, R. J. P. Williams, 637. The stability of transition-metal complexes. *J. Chem. Soc.*, 3192–3210 (1953), 10.1039/JR9530003192.
28. A. W. Varnes, R. B. Dodson, E. L. Wehry, Interactions of transition-metal ions with photoexcited states of flavines. Fluorescence quenching studies. *J. Am. Chem. Soc.* **94**, 946–950 (1972).
29. J. A. Kemlo, T. M. Shepherd, Quenching of excited singlet states by metal ions. *Chem. Phys. Lett.* **47**, 158–162 (1977).
30. A. T. Aron, A. G. Reeves, C. J. Chang, Activity-based sensing fluorescent probes for iron in biological systems. *Curr. Opin. Chem. Biol.* **43**, 113–118 (2018).
31. K. J. Bruemmer, S. W. M. Crossley, C. J. Chang, Activity-based sensing: A synthetic methods approach for selective molecular imaging and beyond. *Angew. Chem. Int. Ed. Engl.* **59**, 13734–13762 (2020).
32. S. D. Fontaine, A. G. DiPasquale, A. R. Renslo, Efficient and stereocontrolled synthesis of 1,2,4-Trioxolanes useful for ferrous iron-dependent drug delivery. *Org. Lett.* **16**, 5776–5779 (2014).
33. B. Spangler *et al.*, A reactivity-based probe of the intracellular labile ferrous iron pool. *Nat. Chem. Biol.* **12**, 680–685 (2016).
34. A. T. Aron, M. O. Loehr, J. Bogena, C. J. Chang, An endoperoxide reactivity-based FRET probe for ratiometric fluorescence imaging of labile iron pools in living cells. *J. Am. Chem. Soc.* **138**, 14338–14346 (2016).
35. A. T. Aron *et al.*, In vivo bioluminescence imaging of labile iron accumulation in a murine model of Acinetobacter baumannii infection. *Proc. Natl. Acad. Sci. U.S.A.* **114**, 12669–12674 (2017).
36. R. K. Muir *et al.*, Measuring dynamic changes in the labile iron pool in vivo with a reactivity-based probe for positron emission tomography. *ACS Cent. Sci.* **5**, 727–736 (2019).
37. R. L. Gonciarz *et al.*, In vivo bioluminescence imaging of labile iron in xenograft models and liver using FeAL-1, an iron-activatable form of D-luciferin. *Cell Chem. Biol.* **30**, 1468–1477.e6 (2023).
38. R. L. Gonciarz, E. A. Collisson, A. R. Renslo, Ferrous iron-dependent pharmacology. *Trends Pharmacol. Sci.* **42**, 7–18 (2021).
39. Ning Zhao *et al.*, Ferronostics: Measuring tumoral ferrous iron with PET to predict sensitivity to iron-targeted cancer therapies. *J. Nucl. Med.* **62**, 949 (2021).
40. T. Hirayama, K. Okuda, H. Nagasawa, A highly selective turn-on fluorescent probe for iron(ii) to visualize labile iron in living cells. *Chem. Sci.* **4**, 1250–1256 (2013).
41. M. Niwa, T. Hirayama, K. Okuda, H. Nagasawa, A new class of high-contrast Fe(ii) selective fluorescent probes based on spirocyclized scaffolds for visualization of intracellular labile iron delivered by transferrin. *Org. Biomol. Chem.* **12**, 6590–6597 (2014).
42. T. Hirayama *et al.*, A universal fluorogenic switch for Fe(ii) ion based on N-oxide chemistry permits the visualization of intracellular redox equilibrium shift towards labile iron in hypoxic tumor cells. *Chem. Sci.* **8**, 4858–4866 (2017).
43. M. Niwa, T. Hirayama, I. Oomoto, D. O. Wang, H. Nagasawa, Fe(II) ion release during endocytotic uptake of iron visualized by a membrane-anchoring Fe(II) fluorescent probe. *ACS Chem. Biol.* **13**, 1853–1861 (2018).
44. T. Hirayama, S. Kadota, M. Niwa, H. Nagasawa, A mitochondria-targeted fluorescent probe for selective detection of mitochondrial labile Fe(ii). *Metallomics* **10**, 794–801 (2018).
45. T. Hirayama *et al.*, A Golgi-targeting fluorescent probe for labile Fe(ii) to reveal an abnormal cellular iron distribution induced by dysfunction of VPS35. *Chem. Sci.* **10**, 1514–1521 (2019).
46. K. Kawai *et al.*, Molecular imaging of labile heme in living cells using a small molecule fluorescent probe. *J. Am. Chem. Soc.* **144**, 3793–3803 (2022).
47. S. Maiti, Z. Aydin, Y. Zhang, M. Guo, Reaction-based turn-on fluorescent probes with magnetic responses for Fe2+ detection in live cells. *Dalton Trans.* **44**, 8942–8949 (2015).
48. H. Y. Au-Yeung, J. Chan, T. Chantarojsiri, C. J. Chang, Molecular imaging of labile iron(II) pools in living cells with a turn-on fluorescent probe. *J. Am. Chem. Soc.* **135**, 15165–15173 (2013).
49. Y.-C. Chen *et al.*, Reactivity-based probe of the iron(II)-dependent interactome identifies new cellular modulators of ferroptosis. *J. Am. Chem. Soc.* **142**, 19085–19093 (2020).
50. M. Chiba *et al.*, Activatable photosensitizer for targeted ablatiOn of lacz-positive cells with single-cell resolution. *ACS Cent. Sci.* **5**, 1676–1681 (2019).
51. H. Zhu *et al.*, Imaging and profiling of proteins under oxidative conditions in cells and tissues by hydrogen-peroxide-responsive labeling. *J. Am. Chem. Soc.* **142**, 15711–15721 (2020).
52. H. Iwashita, E. Castillo, M. S. Messina, R. A. Swanson, C. J. Chang, A tandem activity-based sensing and labeling strategy enables imaging of transcellular hydrogen peroxide signaling. *Proc. Natl. Acad. Sci. U.S.A.* **118**, e2018513118 (2021).
53. S. Uchinomiya *et al.*, Fluorescence-based detection of fatty acid β-oxidation in cells and tissues using quinone methide-releasing probes. *J. Am. Chem. Soc.* **145**, 8248–8260 (2023).
54. E. Kisin-Finfer, S. Ferber, R. Blau, R. Satchi-Fainaro, D. Shabat, Synthesis and evaluation of new NIR-fluorescent probes for cathepsin B: ICT versus FRET as a turn-ON mode-of-action. *Bioorg. Med. Chem. Lett.* **24**, 2453–2458 (2014).
55. A. Dal Corso, L. Pignataro, L. Belvisi, C. Gennari, Innovative linker strategies for tumor-targeted drug conjugates. *Chem. A Eur. J.* **25**, 14740–14757 (2019).
56. B. R. Blank *et al.*, Antimalarial trioxolanes with superior drug-like properties and in vivo efficacy. *ACS Infect. Dis.* **6**, 1827–1835 (2020).
57. C. Chen, B. H. Paw, Cellular and mitochondrial iron homeostasis in vertebrates. *Biochim. Biophys. Acta* **1823**, 1459–1467 (2012).
58. S. Levi *et al.*, Mechanism of ferritin iron uptake: Activity of the H-chain and deletion mapping of the ferro-oxidase site. A study of iron uptake and ferro-oxidase activity of human liver, recombinant H-chain ferritins, and of two H-chain deletion mutants. *J. Biol. Chem.* **263**, 18086–18092 (1988).
59. J. D. Mancias, X. Wang, S. P. Gygi, J. W. Harper, A. C. Kimmelman, Quantitative proteomics identifies NCOA4 as the cargo receptor mediating ferritinophagy. *Nature* **509**, 105–109 (2014).
60. J. D. Mancias *et al.*, Ferritinophagy via NCOA4 is required for erythropoiesis and is regulated by iron dependent HERC2-mediated proteolysis. *Elife* **4**, e10308 (2015).
61. J. M. Goodwin *et al.*, Autophagy-independent lysosomal targeting regulated by ULK1/2-FIP200 and ATG9. *Cell Rep.* **20**, 2341–2356 (2017).
62. N. Santana-Codina *et al.*, NCOA4-mediated ferritinophagy is a pancreatic cancer dependency via maintenance of iron bioavailability for iron-sulfur cluster proteins. *Cancer Discov.* **12**, 2180–2197 (2022).
63. T. Ohshima, H. Yamamoto, Y. Sakamaki, C. Saito, N. Mizushima, NCOA4 drives ferritin phase separation to facilitate macroferritinophagy and microferritinophagy. *J. Cell Biol.* **221**, e202203102 (2022).
64. P. Moi, K. Chan, I. Asunis, A. Cao, Y. W. Kan, Isolation of NF-E2-related factor 2 (Nrf2), a NF-E2-like basic leucine zipper transcriptional activator that binds to the tandem NF-E2/AP1 repeat of the beta-globin locus control region. *Proc. Natl. Acad. Sci. U.S.A.* **91**, 9926–9930 (1994).
65. M. J. Kerins, A. Ooi, The roles of NRF2 in modulating cellular iron homeostasis. *Antioxid. Redox Signaling* **29**, 1756–1773 (2018).
66. A. Anandhan *et al.*, NRF2 controls iron homeostasis and ferroptosis through HERC2 and VAMP8. *Sci. Adv.* **9**, eade9585 (2023).
67. K. Itoh *et al.*, Keap1 represses nuclear activation of antioxidant responsive elements by Nrf2 through binding to the amino-terminal Neh2 domain. *Genes Dev.* **13**, 76–86 (1999).
68. M.-K. Kwak, K. Itoh, M. Yamamoto, T. W. Kensler, Enhanced expression of the transcription factor Nrf2 by cancer chemopreventive agents: Role of antioxidant response element-like sequences in the nrf2 promoter. *Mol. Cell. Biol.* **22**, 2883–2892 (2002).
69. J. D. Hayes, M. McMahon, NRF2 and KEAP1 mutations: Permanent activation of an adaptive response in cancer. *Trends Biochem. Sci.* **34**, 176–188 (2009).
70. G. M. DeNicola *et al.*, Oncogene-induced Nrf2 transcription promotes ROS detoxification and tumorigenesis. *Nature* **475**, 106–109 (2011).
71. M. B. Sporn, K. T. Liby, NRF2 and cancer: The good, the bad and the importance of context. *Nat. Rev. Cancer* **12**, 564–571 (2012).
72. I. S. Harris, G. M. DeNicola, The complex interplay between antioxidants and ROS in cancer. *Trends Cell Biol.* **30**, 440–451 (2020).
73. Q. Guo *et al.*, The role of iron in cancer progression. *Front. Oncol.* **11**, 778492 (2021).
74. R. D. Horniblow *et al.*, Iron-mediated epigenetic activation of NRF2 targets. *J. Nutr. Biochem.* **101**, 108929 (2022).
75. X. Yu *et al.*, Inhibition of NRF2 enhances the acute myeloid leukemia cell death induced by venetoclax via the ferroptosis pathway. *Cell Death Discov.* **10**, 35 (2024).
76. Y. P. Kang *et al.*, Cysteine dioxygenase 1 is a metabolic liability for non-small cell lung cancer. *Elife* **8**, e45572 (2019).
77. M. Gong *et al.*, Loss-of-function mutations in KEAP1 drive lung cancer progression via KEAP1/NRF2 pathway activation. *Cell Commun. Signaling* **18**, 98 (2020).
78. Y. R. Kim *et al.*, Oncogenic NRF2 mutations in squamous cell carcinomas of oesophagus and skin. *J. Pathol.* **220**, 446–451 (2010).
79. G. M. DeNicola *et al.*, NRF2 regulates serine biosynthesis in non-small cell lung cancer. *Nat. Genet.* **47**, 1475–1481 (2015).
80. C. Jiang *et al.*, A CRISPR screen identifies redox vulnerabilities for KEAP1/NRF2 mutant non-small cell lung cancer. *Redox Biol.* **54**, 102358 (2022).
81. T. Hirayama, M. Niwa, S. Hirosawa, H. Nagasawa, High-throughput screening for the discovery of iron homeostasis modulators using an extremely sensitive fluorescent probe. *ACS Sens.* **5**, 2950–2958 (2020).
82. L. Zhang *et al.*, Nrf2 is a potential modulator for orchestrating iron homeostasis and redox balance in cancer cells. *Front. Cell and Dev. Biol.* **9**, 728172 (2021).
83. Y. P. Kang *et al.*, Non-canonical glutamate-cysteine ligase activity protects against ferroptosis. *Cell Metab.* **33**, 174–189.e7 (2021).
84. C. J. Chang, Searching for harmony in transition-metal signaling. *Nat. Chem. Biol.* **11**, 744–747 (2015).